Title: *Sleeping Beauty* insertional mutagenesis reveals important genetic drivers of central nervous system embryonal tumors.

Authors: Pauline J. Beckmann (co-first)[1], Jon D. Larson (co-first)[1], Alex T. Larsson[1], Jason P. Ostergaard[1], Sandra Wagner[1], Eric P. Rahrmann[1,2], Ghaidan A. Shamsan[3], George M. Otto[1,4], Rory L. Williams[1,5], Jun Wang[6], Catherine Lee[6], Barbara R. Tschida[1], Paramita Das[1], Adrian M. Dubuc[7], Branden S. Moriarity[1], Daniel Picard[8], Xiaochong Wu[9], Fausto J. Rodriguez[10], Quincy Rosemarie[1,11], Ryan D. Krebs[1], Amy M. Molan[1,12], Addison M. Demer[1], Michelle M. Frees[1], Anthony E. Rizzardi[13], Stephen C. Schmechel[13,14], Charles G. Eberhart[15], Robert B. Jenkins[16], Robert J. Wechsler-Reya[6], David J. Odde[4], Annie Huang[17], Michael D. Taylor[11], Aaron L. Sarver[1], David A. Largaespada[1*].

[1]Masonic Cancer Center, Department of Pediatrics, and Center for Genome Engineering, University of Minnesota, Minneapolis, MN 55455, USA. [2]Cancer Research UK, Cambridge Institute, University of Cambridge, Cambridge, England CB2 0RE, UK. [3]Department of Biomedical Engineering, University of Minnesota, Minneapolis, MN 55455, USA. [4]Department of Molecular and Cellular Biology, University of California, Berkeley, Berkeley, California, 94720-3200, USA. [5]Department of Bioengineering, California Institute of Technology, Pasadena, California, 91125, USA. [6]Tumor Initiation and Maintenance Program, NCI-Designated Cancer Center, Sanford Burnham Prebys Medical Discovery Institute, La Jolla, CA 92037, USA. [7]Department of Pathology, Brigham and Women's Hospital, Harvard Medical School, Boston, MA 02115, USA. [8]Department of Pediatric Neuro-Oncogenomics, German Cancer Research Center (DKFZ) and German Cancer Consortium (DKTK), Heidelberg, Germany; and Department of Pediatric Oncology, Hematology, and Clinical Immunology, Medical Faculty, University Hospital Düsseldorf, Düsseldorf, Germany. [9]Division of Neurosurgery, Arthur and Sonia Labatt Brain Tumor Research Center, The Hospital for Sick Children, Toronto, Ontario, Canada M5G1X8. [10]Division of Neuropathology, Johns Hopkins Hospital, Baltimore, MD 21231, USA. [11]McArdle Laboratory for Cancer Research, University of Wisconsin-Madison, Madison, WI 53705, USA. [12]Department of Biochemistry, Molecular Biology, and Biophysics, University of Minnesota, Minneapolis, MN 55455, USA. [13]Department of Laboratory Medicine and Pathology, University of MN, Minneapolis, MN 55455, USA. [14]Department of Clinical Sciences, College of Medicine, Florida State University, Sarasota, FL 34236, USA. [15]Department of Pathology, Ophthalmology and Oncology, The Johns Hopkins University School of Medicine, Baltimore, Maryland 21287, USA. [16]Department of Laboratory Medicine and Pathology, Mayo Clinic and Foundation, 200 First Street Southwest, Rochester, Minnesota 55905, USA. [17]Division of Hematology, The Hospital for Sick Children, Toronto, Ontario, Canada M5G1X8

Running title: *SB* identifies novel drivers in medulloblastoma and CNS-PNET.

Keywords: SB, Medulloblastoma, CNS-PNET, Arhgap36, Foxr2

Financial support: Support for this research was provided by The American Cancer Society (Research Professor Award #123939 to DAL), the National Institutes of Health (U54CA210190 to DAL and DJO, R01CA113636 to DAL, T32 T32GM113846 to PJB, R50-

CA211249 to ALS, T32 AI083196 to BRT, T32CA009138 to JDL, and R01CA172986 to DJO), the Children's Cancer Research Fund, and the Hedberg Family Chair (to DAL).

Correspondence:
David A. Largaespada
Address: Cancer and Cardiovascular Research Building
1st Floor Mailroom CCRB
2812A 2231 6th St SE
Minneapolis, MN 55455 USA
Email: larga002@umn.edu
Telephone: 612-626-4979
Fax: 612-624-3869

Disclosures: DAL is the co-founder and co-owner of several biotechnology companies including NeoClone Biotechnologies, Inc., Discovery Genomics, Inc. (recently acquired by Immunsoft, Inc.), and B-MoGen Biotechnologies, Inc. He consults for Surrogen, Inc. Genentech, Inc. is funding some of his research. The business of all these companies is unrelated to the contents of this manuscript. Other authors have no conflicts of interest.

*manuscript includes 4989 words, 7 main figures, 7 supplementary figures, and 9 supplementary tables

Abstract

Medulloblastoma and central nervous system primitive neuroectodermal tumors (CNS-PNET) are aggressive, poorly differentiated brain tumors with limited effective therapies. Using *Sleeping Beauty* (*SB*) transposon mutagenesis, we identified novel genetic drivers of medulloblastoma and CNS-PNET. Cross-species gene expression analyses classified SB-driven tumors into distinct medulloblastoma and CNS-PNET subgroups, indicating they resemble human SHH and group 3 and 4 medulloblastoma and CNS neuroblastoma with *FOXR2* activation. This represents the first genetically-induced mouse model of CNS-PNET and a rare model of group 3 and 4 medulloblastoma. We identified several putative proto-oncogenes including *Arhgap36*, *Megf10*, and *Foxr2*. Genetic manipulation of these genes demonstrated a robust impact on tumorigenesis *in vitro* and *in vivo*. We also determined that FOXR2 interacts with N-MYC, increases C-MYC protein stability, and activates FAK/SRC signaling. Altogether, our study identified several promising therapeutic targets in medulloblastoma and CNS-PNET.

Significance

A transposon-induced mouse model identifies several novel genetic drivers and potential therapeutic targets in medulloblastoma and CNS-PNET.

Introduction

Embryonal tumors, including medulloblastoma and central nervous system primitive neuroectodermal tumors (CNS-PNETs), represent the most common malignant pediatric brain tumors (1). For ease of historical comparison, CNS-PNET is used in this manuscript according to the 2007 World Health Organization CNS tumor classification and includes CNS neuroblastomas, CNS ganglioneuroblastomas, medulloepitheliomas, and ependymoblastomas, although CNS-PNET no longer exists as an umbrella term(2). Medulloblastoma and CNS-PNET have similar histology: densely-packed, small cells with hyperchromatic nuclei and little cytoplasm. Medulloblastomas are usually cerebellar, while CNS-PNETs occur predominantly in the cerebrum. Aggressive, multi-modality treatments improve survival but produce lifelong side effects, and 5-year survival rates remain 60-65% for medulloblastoma and 20-40% for CNS-PNET(3).

Medulloblastoma and CNS-PNET are molecularly heterogenous. Medulloblastoma includes four molecular subgroups: WNT, SHH, group 3, and group 4; WNT and SHH are associated with mutations activating those pathways, but groups 3 and 4 remain less defined(4). A genomic study by Picard *et al*. identified three distinct CNS-PNET subgroups: primitive-neural, oligo-neural, and mesenchymal(5). Using methylation and gene expression-based analyses, Sturm *et al*. identified 4 molecular subgroups of CNS-PNET associated with gene fusions(6). While our understanding of the tumor biology has improved, a lack of animal models and targetable oncogenic drivers impede therapeutic development, particularly in group 3/4 medulloblastoma and CNS-PNET.

We used *Sleeping Beauty* (*SB*) transposon mutagenesis to identify novel medulloblastoma and CNS-PNET drivers. Transposition initiated in neural progenitor cells using *Nestin*-Cre was used alone, with *Trp53*$^{lsl\text{-}R270H/+}$, or with *Pten*-deficiency to generate medulloblastomas and CNS-PNETs. These tumors resembled human medulloblastoma and CNS-PNET histologically and transcriptionally. Three candidate oncogenes, *Arhgap36*, *Foxr2*, and *Megf10* were validated *in vitro* and *in vivo* and their mechanisms examined.

Materials and Methods

Generation of transgenic mice

Animal studies were conducted using procedures approved and monitored by the Institutional Animal Care and Use Committee at the University of Minnesota (UofMN). *Nestin-Cre* mice(7) were bred to either *T2/Onc* (chromosome 1/15)(8) or *T2/Onc2* (chromosome 4)(9) to generate *Nestin-Cre*:*T2/Onc(2)*. *Rosa26*$^{lsl\text{-}SB11/+}$(10) were bred to either *Trp53*$^{lsl\text{-}R270H/+}$(11) or *Pten*$^{flox/flox}$(12) to generate *Rosa26*$^{lsl\text{-}SB11/+}$:*Pten*$^{flox/flox}$ or *Rosa26*$^{lsl\text{-}SB11/+}$:*Trp53*$^{lsl\text{-}R270H/+}$. *Nestin-Cre*:*T2/Onc(2)* mice were bred to *Rosa26*$^{lsl\text{-}SB11/+}$:*Pten*$^{flox/flox}$ or *Rosa26*$^{lsl\text{-}SB11/+}$:*Trp53*$^{lsl\text{-}R270H/+}$ to generate mice with and without CNS-restricted *SB*-mutagenesis on wildtype (WT), *Trp53*$^{lsl\text{-}R270H/+}$, and *Pten*$^{flox/+}$ backgrounds. *T2/Onc(2)* excision PCR was performed as described with primers in Supplementary Table 1(8).

Immunohistochemistry (IHC), immunoprecipitation (IP), and western blotting

Unstained tissue microarray (TMA) sections of formalin-fixed, paraffin-embedded (FFPE) human tumor specimens were obtained through the UofMN Materials Procurement Network (11

samples) and Johns Hopkins University (54 samples). FFPE tissue slides were stained with Hematoxylin and Eosin (H&E) or IHC using standard methods. IPs were done (Active Motif #54001) with 500μg total protein. Western blotting was done with whole cell lysates as described(13) using antibodies in Supplementary Table 2.

DNA-Common insertion site (D-CIS) analysis
Linker-mediated PCR to identify transposon insertion sites was performed as described(13). Transposon insertion sites were annotated using TAPDANCE(14). Non-redundant insertion sites representing >0.1% of the mapped insertions from each tumor library were used to generate CIS (*P*-value <0.05).

Transcriptional profiling
Isolated tumor RNA (Qiagen #75114) was assessed for quality using capillary electrophoresis (RIN>6.5, Agilent 2100 BioAnalyzer). Paired-end sequencing (30-40 million reads/sample) of TruSeq-prepared libraries was performed (Illumina HiSeq 2000). Raw FASTQ files are available at the NCBI Sequence Read Archive and linked to Gene Expression Omnibus SuperSeries (GSE122050). FASTQ files were mapped to the MM10 genome (*T2/Onc* and *Rosa26*$^{lsl\text{-}SB11/+}$ as additional chromosomes)(15) using STAR-Fusion (https://github.com/STAR-Fusion/STAR-Fusion/wiki). Transcript FPKM values were computed using cuffquant and cuffnorm and adjusted by +0.1(16).

T2/Onc fusion identification
To identify *T2/Onc*:genome fusions, we analyzed the chimeric.out.junction and chimeric.out.sam output files from STAR-Fusion to summarize the number of junction (one read contains the *T2/Onc*:genome junction) and bridge (one paired-end read maps to *T2/Onc* and the other to the genome) reads present within 1000bp regions. Fusions supported by ≥1 junction read or ≥3 bridging reads were retained for analysis. Manual detection of *T2/Onc(2):Arhgap36* transcripts was done using 500ng of purified RNA (Invitrogen #15596-018), reverse-transcribed (Invitrogen #18080-051) and amplified using primers in Supplementary Table 1.

Gene cluster similarity (GC-SIM)
GC-SIM was used for unsupervised, unbiased identification of similar gene clusters across transcriptional datasets. Transcriptional profile datasets were individually log-transformed, mean-centered, filtered for highly variant genes, and hierarchically clustered using average linkage and (1 – Pearson correlation) as the distance metric. Gene clusters with node correlation and size >respective thresholds were retained. Cross-dataset cluster pairs were tested for enrichment of common gene members (Fisher's Exact Test) to identify conserved transcriptional patterns.

RT-PCR and 5′-rapid amplification of cDNA ends (5'-RACE)
For CNS-PNET expression analysis, cDNAs were synthesized (Applied Biosystems #4368814) and qRT-PCR was performed (Invitrogen #4369016). For Shh activation assays, purified cellular RNA (Ambion #12183025) was reverse transcribed (Invitrogen #11755050) and qRT-PCR was done in triplicate (Roche #4673492001). Shh activation was done as described(17). For 5'-RACE (Ambion #AM1700), tumor RNA was extracted from human medulloblastomas (Invitrogen #15596-018) and normal human brain RNA was purchased from BioChain

(R1244039-50, R1244035-50, R1234040-10). Subsequent detection of transcripts by RT-PCR was performed with 500ng RNA (Invitrogen #18080-051). Primers and probes are listed in Supplementary Table 1.

Cell culture/assays

Cell lines were maintained, authenticated, and tested for mycoplasma as described in Supplementary Table 3. MTS (Promega G1111), soft agar assays, and transfections were done as described(13). Stable lines transfected with cDNAs (*ARHGAP36* (Q6ZRI8-5), *FOXR2* (Q6PJQ5-1), *Megf10* (Q6DIB5-1)) were cultured as polyclonal populations in puromycin. Transient transfection in HEK293Ts was done per manufacture's protocol (Invitrogen 11668019). CRISPR-KO clones were isolated as described(13). Briefly, Daoy cells were transfected with PiggyBAC transposase and a puromycin-selectable PiggyBAC transposon vector containing 2 *FOXR2* guide RNAs (sequences in Supplementary Table 1) and Cas9. Isolated clones were sequenced to identify changes in *FOXR2*. Wound healing assays were performed as described(18). Primary granule neuron precursors (GNPs) were isolated from neonatal C57BL/6J and thymidine incorporation assays were performed as described(19).

in vivo assays

NRG mice (Jackson 007799) were injected as described(20). Briefly, C17.2 cells were prepared in HBSS, counted, and stored on ice prior to injection ($2x10^5$ cells/2µl injection). P0 mice were injected in the fourth ventricle (stereotactic coordinates: 1.5mm anterior to Bregma, 1.5mm deep). Successful injection was verified on P1 by luciferase imaging as described(20). Adult intracranial injections were performed as described(19). Female NU/J mice (Jackson 002019, 6-8 weeks old) were anesthetized (81 mg/kg ketamine, 13.8 mg/kg xylazine) and injected with $1x10^6$ cells/5µl (prepared as above). For flank tumor assays, female NU/J mice (Jackson 002019, 6-8 weeks old) were injected with $1x10^6$ C17.2 cells (prepared as above) resuspended 1:1 in HBSS and Matrigel (Corning CB-#40234C). Tumor volume = (l x w^2)/2, l=length and w=width.

Results

SB Mutagenesis Promotes Medulloblastoma and CNS-PNET Formation

To identify genetic drivers of medulloblastoma and CNS-PNET, we targeted Nestin+ neural and glial precursor cells with *SB*-mutagenesis on three genetic backgrounds: wildtype (WT), *Pten* heterozygous (*Pten*$^{flox/+}$), or *Trp53* mutant (*Trp53*$^{lsl\text{-}R270H/+}$). *Pten*$^{flox/+}$ and *Trp53*$^{lsl\text{-}R270H/+}$ served as sensitizing backgrounds as they are mutated in human medulloblastoma and CNS-PNET(21,22). IHC revealed SB expression throughout the developing brain, including cells within the granule layer, white matter, surrounding the fourth ventricle, subependymal midbrain, subventricular zone, and olfactory bulb (Supplementary Fig. S1A-G). Experimental cohorts harbored one of three transposon concatemers (Supplementary Fig. S1H). *SB*-mutagenesis significantly reduced survival in combination with *Trp53*$^{lsl\text{-}R270H}$ (Supplementary Fig. S1I-K). Upon necropsy we observed masses in the brain, testicles, bone, peripheral lymph nodes, and spleen (Supplementary Fig. S1I-K, Supplementary Table 4).

Histological analysis of brain masses revealed the presence of infratentorial medulloblastoma and supratentorial CNS-PNET (22 medulloblastomas and 14 CNS-PNETs) with highest medulloblastoma frequency in *Trp53*$^{lsl\text{-}R270H/+}$ mice (Fig. 1A-B). The high-copy transposon (*T2Onc2*, chromosome 4) produced the highest proportion of medulloblastoma, while

CNS-PNETs were equally derived from chromosome 4 and 15 concatemers (Supplementary Fig. S2A). Tumors expressed nuclear SB by IHC and showed transposon mobilization by PCR (Supplementary Fig. S2B-C).

SB-Induced Medulloblastoma and CNS-PNET Resemble Human Tumors Histologically

SB-induced medulloblastomas originated in the cerebellum whereas CNS-PNETs occurred in the rostral portion of the brain, overwhelming the olfactory bulbs, lateral ventricle, and cortex (Fig. 1A, C-D). Both tumor types resembled their human counterparts histologically (small round cells with high nuclear:cytoplasmic ratios, Homer-Wright rosettes, vascularization, and mitotic figures), expressed diagnostic markers for human medulloblastoma and CNS-PNET (Synaptophysin, Ki67, and Nestin), and stained negatively for the astrocytic marker Gfap (Fig. 1C-D). 50% of medulloblastomas and 100% of CNS-PNETs exhibited metastatic characteristics, including infiltration into the leptomeninges, parenchyma, brainstem, and cortex (Supplementary Table 4). Leptomeningeal spread is of interest due to its associated poor prognosis, prevalence (one-third of patients), and difficulty modeling(5,23).

SB-Induced Medulloblastomas Resemble Non-WNT Human Medulloblastoma

We transcriptionally profiled 18 *SB*-induced medulloblastomas, revealing two clear subgroups that each matched human medulloblastoma subtypes (Fig. 2A)(6). The first subgroup (N=13) showed increased *Gli1*, canonically associated with human SHH medulloblastoma(24). The second subgroup (N=5) showed increased *Npr3* and *Kcna1*, markers for human group 3 and 4, respectively(24). More globally, the *Gli1*-overexpressing medulloblastoma gene set overlapped with highly-expressed genes in human SHH medulloblastoma (N=48, Fig. 2A, Supplementary Table 5)(6). Similarly, the *Npr3* and *Kcna1*-overexpressing mouse gene set overlapped with highly-expressed genes in human group 3 and 4 medulloblastoma (N=120). Mouse tumors did not exhibit Wnt signatures.

SB-Induced CNS-PNETs Resemble Human CNS Neuroblastoma with FOXR2 Activation (CNS NB-FOXR2)

Transcriptional profiling comparing mouse CNS-PNETs (N=5) to published human CNS-PNETs (N=58) revealed two subgroups (Fig. 2B)(6). A single cluster of co-varying genes (N=298) was significantly enriched in both human and mouse CNS-PNET and contained high levels of CNS NB-*FOXR2* associated genes, including *MMP24*, *KCJN9*, and *CHGB* (Fig. 2B, Supplementary Table 6). Consistent with CNS NB-*FOXR2* classification, *SB*-induced CNS-PNETs showed significantly increased *Olig1*, *Olig2*, and *Sox10* by qPCR and were Olig2+ by IHC (Supplementary Fig. 2D-E). The three remaining mouse CNS-PNETs had elevated expression of CNS EFT-*CIC* marker genes (*Shc4*, *Argdib*, and *Pole*) but no clearly corresponding human subgroup.

CIS reveal candidate cancer genes

We performed linker-mediated PCR on 22 medulloblastomas and 13 CNS-PNETs and identified 390,000 and 155,000 non-redundant insertions, respectively. TAPDANCE analysis(14) identified 13 medulloblastoma and 15 CNS-PNET DNA-CIS (D-CIS)(Fig. 3A, Supplementary Table 7). We also identified RNA-CIS (R-CIS) in both tumor types, defined as transposon fusion transcripts present in both ≥10% of cases and ≥1 tumor (Fig. 3A, Supplementary Table 7). For several putative oncogenes, the presence of a *T2/Onc(2)* fusion

transcript significantly increased expression (Fig. 3B). We identified genes previously implicated in medulloblastoma, including *Gli1* and *Pten*; upregulation of *GLI1* expression and PI3K pathway activation through *PTEN* loss are observed in human medulloblastoma(21). Predicted transposon-mediated driving effects on Gli1 expression were confirmed by IHC (Supplementary Fig. S3A). We also confirmed Pten reduction and a corresponding increase in pAkt with *Pten* insertions (Supplementary Fig. 3B). *Arhgap36* was most frequently modified, with insertions identified in 14 (D-CIS) and 13 (R-CIS) medulloblastomas and 2 CNS-PNETs (R-CIS). *Enox2*, a tumor-associated NADH oxidase involved in the growth of several cancer cell lines(25), was also a D and R-CIS in medulloblastoma (predicted *SB* oncogene).

We identified known and novel molecular changes in *SB*-induced CNS-PNETs. *Pten* was a predicted tumor suppressor gene (TSG) and loss of *PTEN* through 10q loss or mutation is observed in human CNS-PNET(22). Novel to this study, *NF1* was the most targeted CNS-PNET TSG. We identified several other predicted Ras effector gene alterations, including *Eras* overexpression and *Erbb2ip* and *Rasa3* disruption (Supplementary Table 4). Tumors harboring these insertions exhibited increased pErk (Supplementary Fig. S3C, Supplementary Table 4) supporting Ras pathway activation. We also observed *NF1* locus deletion in a subset of human CNS-PNETs (Supplementary Fig. S3D).

We next analyzed our CIS gene expression in published human medulloblastomas and CNS-PNETs (Fig. 3C-E)(6). *GRIA4* showed high expression in both SHH medulloblastoma and CNS NB-*FOXR2*. *FOXR2* is elevated in a subset of WNT medulloblastoma and CNS NB-*FOXR2*. Interestingly, *ARHGAP36* is highly expressed in group 3 and 4 medulloblastoma, with low expression in SHH (Supplementary Fig. S4A), while in the mouse *Arhgap36* insertions occurred in Shh and group 3/4 tumors (7/12 Shh and 4/5 group 3/4 tumors, Supplementary Table 4).

ARHGAP36 Expression is Associated with Poor Prognosis in Human Medulloblastoma

Transposon location and orientation implicate *Arhgap36* as an oncogene, with insertions upstream of the locus or within intron 1 and significantly increasing gene expression (Fig. 4A-B). *T2/Onc:Arhgap36* transcripts displayed precise fusion of the *T2/Onc* splice donor to the *Arhgap36* exon 2 splice acceptor (Supplementary Fig. S4B), generating a 15 amino acid N-terminal truncation with translation from an in-frame ATG. Tumors with *Arhgap36* insertions showed high levels of cytoplasmic Arhgap36 by IHC compared to tumors without *Arhgap36* insertions, which displayed sparse nuclear expression similar to normal granule cells (Fig. 4C). Spatial and temporal analysis of ARHGAP36 expression in normal human and mouse cells within developing and mature cerebella showed nuclear localization throughout the molecular layer (ML), Purkinje cell layer (PC) and internal granule cell layer (IGL)(Supplementary Fig. S4C). In two combined TMAs of human medulloblastoma, 37/65 (56%) and 8/65 (12%) expressed cytoplasmic and nuclear ARHGAP36 expression, respectively, by IHC (Fig. 4D). ARHGAP36 protein was expressed across all human subgroups, although increased *ARHGAP36* transcript was only expressed in group 3/4 human medulloblastoma (Fig. 4E, Supplementary Fig. S4A)(24). Overall and cytoplasmic ARHGAP36 expression correlated with accelerated mortality (Fig. 4F, Supplementary Fig. S4D).

We further investigated *ARHGAP36* transcript profiles using 5′-RACE on human group 3/4 medulloblastoma samples, cell lines, and normal cerebellar cells. Several *ARHGAP36* amplification products were identified (Supplementary Fig. 4E-F) predicting expression of canonical isoform 1(*), 5(**), and 3(***; ****). All 3 isoforms contain intact ARHGAP36

predicted functional domains, including an arginine-rich domain (ARR), nuclear localization sequence (NLS), and GTPase-activating protein (GAP) domain. Interestingly, the 5' ends of *** and **** begin with intron 2 sequences splicing to exon 3 and an in-frame ATG located in exon 4. Target-specific RT-PCR revealed these *ARHGAP36* sequences in additional tumor samples, while normal fetal cerebellum only expressed isoform 1 (Supplementary Fig. S4G).

ARHGAP36 Promotes Tumor Formation in Neural Progenitor Cells

To further characterize the role of ARHGAP36 in medulloblastoma, we overexpressed truncated *ARHGAP36* (isoform 5) in the mouse neural progenitor cell line C17.2 (Supplementary Fig. 5A)(26). Increased ARHGAP36 significantly enhanced soft agar colony formation but did not affect proliferation or collective cell migration rate (Fig. 5A, Supplementary Fig. S5B-C). C17.2 cells expressing ARHGAP36 formed tumors significantly faster in the flanks of NU/J mice than luciferase control cells (Fig. 5B). When injected orthotopically into adult NU/J mice, C17.2 cells localized to the granule layer of the cerebellum where ARHGAP36 expression drove leptomeningeal spread into the cerebrum and cerebellar tumor formation, reducing median survival from 99 to 71 days (Fig. 5C-D). Additionally, increased ARHGAP36 expression in primary GNPs significantly increased their proliferation (Fig. 5E). As previously reported, ARHGAP36 strongly activated Shh signaling in C17.2 cells in a ligand-independent manner, providing a potential mechanism for ARHGAP36-driven tumorigenesis (Fig. 5F)(17,27). Additionally, *SB* transposon insertions in the *Arhgap36* locus were mutually exclusive with insertions in *Gli1* and *Gli2*, Shh pathway activators (Fig. 5F).

Megf10 Promotes Transformation in vitro and in vivo

Megf10 (predicted *SB* oncogene) was identified as an R-CIS, with fusion transcripts in 3 medulloblastomas significantly increasing expression (Fig. 3A-B). *Megf10* is expressed throughout the developing CNS and is a positive regulator of Notch signaling(28). *MEGF10* is upregulated in a subset of human CNS-PNET and medulloblastoma (15/26 medulloblastomas, 14/58 CNS-PNETs, Supplementary Fig. S5D). *Megf10* expression in C17.2 cells significantly enhanced colony formation in soft agar, proliferation by MTS, and flank tumor formation (Fig. 5G-I). Additionally, increased *Megf10* expression in GNPs increased their proliferation by 1.7-fold, though not significantly possibly due to low sample size (Fig. 5E). Megf10 had no effect on C17.2 cell Notch signaling, however, by western blot (Supplementary Fig. S5E).

FOXR2 Promotes Transformation in Human and Mouse Cells

All *Foxr2* transposon insertions were located upstream of the translation start site and drove increased *Foxr2* expression, predicting an oncogenic role (Fig. 6A-B). The presence of a *Foxr2* insertion significantly reduced median survival from 166.5 to 116.5 days (Supplementary Fig. S6A). FOXR2 overexpression in C17.2 cells significantly increased soft agar colony formation and collective cell migration without increasing proliferation (Fig. 6C-E, Supplementary Fig. S6B). C17.2 FOXR2 cells formed flank tumors significantly faster than C17.2 Luc controls (Fig. 6F). When injected orthotopically into adult NU/J mice, C17.2 FOXR2 cells migrated to the granule layer of the cerebellum and formed large, vascular tumors, reducing median survival from 99 to 43 days (Supplementary Fig. 6C, Fig. 6G-H). C17.2 FOXR2 cells injected orthotopically into neonatal NRG mice also significantly reduced median survival compared to C17.2 Luc and resulted in tumor formation (110 vs 183 days, Fig. 6I). Importantly, *FOXR2* overexpression drove increased proliferation in primary GNPs (Fig. 5E). Using the

CRISPR/Cas9 system, we knocked out (KO) *FOXR2* in Daoy, a human medulloblastoma cell line. Daoy clone #21 had a nonsense mutation in exon 1 resulting in FOXR2 protein loss, decreased proliferation, and decreased soft agar colony formation, all rescued by *FOXR2* cDNA expression (Fig. 6J-L).

FOXR2 Has a Multi-Faceted Mechanism Including Effects on MYC and FAK

FOXR2 has many suggested oncogenic mechanisms, including interaction with C-MYC(29). We confirmed this interaction by CoIP in a human Schwann cell line, HSC1λ, and C17.2 cells stably expressing *FOXR2* (Fig.7A, Supplementary Fig. 6D). To determine if FOXR2 interacts with other forms of MYC, we transiently transfected HEK293T cells with V5-tagged *C-MYC*, *L-MYC* and *N-MYC*. We observed reduced interaction of FOXR2 with N-MYC and minimal interaction with L-MYC (Fig. 7B). To determine if FOXR2 stabilizes C-MYC, we treated cells with cycloheximide (CHX) to inhibit translation. Almost all C-MYC protein was degraded in control HSC1λ cells, but with FOXR2, C-MYC levels were only reduced by half after 3 hours, indicating FOXR2 is stabilizing (Fig. 7C). Interestingly, C-MYC was highly stable in C17.2 cells regardless of FOXR2 expression, likely due to their immortalization by V-Myc(26), implying that FOXR2 transforms C17.2 cells through alternative mechanisms.

To further characterize the oncogenic mechanism of FOXR2, we synthesized *FOXR2* cDNA constructs missing the following predicted domains: NLS(ΔNLS)(30), MYC interaction (ΔMYC)(29), low complexity regions (ΔLC1, ΔLC2 and ΔLC1/2)(31), and forkhead box transcription factor (ΔTF)(31)(Fig. 7D). We stably expressed each mutant and performed soft agar assays in C17.2 and HSC1λ cells. Surprisingly, no single deletion mutant completely ablated the colony formation promoting capacity of *FOXR2* in either line, but loss of the Myc interaction and LC2 domains significantly reduced colony formation (Fig. 7D, Supplementary Fig. 6E). C17.2 FOXR2ΔMYC also had an intermediate phenotype in the flank (Fig. 6F). We verified that the FOXR2ΔMYC mutant did not bind C-Myc (Supplementary Fig. 6F). Given no single domain loss completely ablated colony formation but some did reduce it, we conclude FOXR2 has a multi-faceted mechanism. We observed a slight change in the actin cytoskeleton of *FOXR2*-expressing cells, prompting assessment of focal adhesion kinase (FAK) activation. C17.2 cells expressing FOXR2 displayed increased Fak phosphorylation (Y397), resulting in increased (activating) phosphorylation at Src Y416 (Fig. 7E). This effect is Myc-independent (Supplementary Fig. 6G). Correspondingly, FOXR2 loss in Daoy cells resulted in decreased pFAK and pSRC rescuable by *FOXR2* cDNA expression (Fig. 7E).

Discussion

We used *SB* transposon mutagenesis to identify novel drivers of medulloblastoma and CNS-PNET. Over half of our D-CIS and several of our R-CIS were reported in previous SB medulloblastoma screens(23,32-34), including *Pten*, *Wac*, *Arid1b, Arhgap36*, *Foxr2*, and *Megf10*, making them especially compelling candidates (Supplementary Table 8). Notably, several R-CIS are located on chromosomes 4 and 15, the locations of the *T2/Onc2* and *T2/Onc* concatemers, respectively. Although local hopping may account for bias toward genes on these chromosomes, several are implicated in cancer, including *Tle1* and *Ptprd* (35,36). Additionally, these concatemers have been previously used to identify R-CIS in osteosarcoma, and only one R-CIS gene was common to both studies (*Cdkn2a*, Supplementary Table 9)(15). Our medulloblastoma R-CIS include several highly compelling targets, including *Megf10*. We

identified a novel, oncogenic role for *Megf10* in neural progenitor cells, the mechanism for which warrants further study.

Ours is the first transposon screen to produce CNS-PNETs. We identified several genes with known roles in neural cancer not previously implicated in CNS-PNET, including *Setd2*, *Ambra1*, and *Usp9x*(37-39). Several Ras-associated genes were mutated in our screen, including *Nf1*, *Eras*, *Pten*, and *Ras3*, suggesting an importance of Ras pathway activation and cooperation with p53 loss in PNETagenesis. Additionally, we identified *NF1* loss in human CNS-PNETs. Activated RAS/MAPK signaling with p53 loss has been shown to drive CNS NB-*FOXR2* formation in zebrafish(40), and somatic *PTEN* loss is associated with human CNS-PNET(22). Interestingly, we did not recover any CNS-PNETs on the *Pten*-deficient background, possibly indicating that p53 loss creates a permissive cell with subsequent Ras activation.

FOXR2 is a member of the forkhead-box (FOX) transcription factor family, which contribute to a wide variety of cellular processes(41). *FOXR2* acts as an oncogene in several neural cancers including: malignant peripheral nerve sheath tumors, glioma, CNS-PNET, and medulloblastoma(6,13,34,42). Interestingly, although *FOXR2* has been shown to be upregulated in CNS NB-*FOXR2*(6), we did not recover *Foxr2* insertions in the *SB*-induced CNS-PNETs, including 2 tumors that resembled CNS NB-*FOXR2* transcriptionally. Other insertions may mimic the CNS NB-*FOXR2* phenotype; these 2 tumors exclusively harbored insertions in *Epb4.1l1*, *Itpr1*, *Rbfox1*, and *Sphkap*.

The mechanism of FOXR2-driven tumorigenesis has proven diverse and elusive. FOXR2 can promote WNT signaling, activate SHH signaling, promote EMT, and affect cell cycle (34,42-45). We examined each of these pathways in C17.2 cells and found no effect of FOXR2 on B-catenin localization, *Axin2*, *Gli1*, *p21*, or *CyclinD1* mRNA expression, or N-Cadherin, E-Cadherin, or Vimentin protein levels (Supplementary Fig. 7A-D). We found that FOXR2 binds and stabilizes C-MYC. Mouse models with C-MYC-driven tumors show an addiction to C-MYC expression, suggesting C-MYC is a strong therapeutic target in cancer(46). However, directly targeting C-MYC has been difficult. Therefore, targeting C-MYC interacting proteins, such as FOXR2, may prove useful for cancer therapy. We also found that FOXR2 promotes activation of the FAK/SRC signaling pathway. FAK activation is associated with poor prognosis and drug resistance in a variety of cancers and targeting FAK produces deleterious off-target effects(47). Interestingly, co-targeting of FAK and C-MYC was recently shown to have synergistic effects in ovarian cancer(48). The ability of FOXR2 to activate both of these pathways makes it an excellent candidate for targeted therapy. Additionally, FOXR2 has minimal expression in adult tissues, making off-target toxicity risk low(13).

We identified *ARHGAP36* as both a mouse and human medulloblastoma oncogene. ARHGAP36 expression in C17.2 cells promoted anchorage independent growth, tumor formation, leptomeningeal spread, and SHH activation. Current therapies targeting an upstream pathway member, Smoothened (SMO), have been met with resistance through SMO mutations(49). Since its interactions with PKA and SUFU are both downstream of SMO, ARHGAP36 poses a good target for treatment-resistant, SHH-driven medulloblastoma(17,27). Additionally, *Arhgap36* was the most up-regulated gene in mouse allografts propagated in the presence of a SMO antagonist(17). Interestingly, *Arhgap36* insertions occurred in mouse Shh and group 3/4 tumors, and *ARHGAP36* is expressed across all subgroups of human medulloblastoma, indicating ARHGAP36 may also have non-SHH pro-tumorigenic effects.

We identified several candidate driver genes in medulloblastoma and CNS-PNET relevant to human cancer. To our knowledge, this is the first study to present a genetically-

induced CNS-PNET mouse model, providing an opportunity for studying this rare and aggressive tumor. We also present tumors that resemble group 3/4 medulloblastoma with high incidence of leptomeningeal spread, again providing a needed mouse model for these tumors. Interestingly, these diverse tumor types were driven with the same, *Nestin*-driven Cre recombinase, indicating that the cell of origin of non-Wnt medulloblastoma and CNS-PNET is Nestin+ or a close descendent. We used RNA-Seq to identify CIS genes and subtype mouse *SB*-induced tumors based on human expression data. *Arhgap36*, our top CIS gene, was shown to transform a mouse neuroblast line. *Foxr2* was identified as a proto-oncogene and shown to promote C-MYC stability and FAK pathway activation. Both of these genes offer promise as novel therapeutic targets in human medulloblastoma and warrant additional study. Further functional testing of additional CIS genes may reveal additional treatment options for embryonal tumors.

Acknowledgements

This work was supported by UofMN Genomics Center, UofMN Biology Materials Procurements Network, Research Animal Resources, and University Imaging Centers that are supported by the National Cancer Institute.

1. Ostrom QT, Gittleman H, Farah P, Ondracek A, Chen Y, Wolinsky Y*, et al.* CBTRUS statistical report: Primary brain and central nervous system tumors diagnosed in the United States in 2006-2010. Neuro Oncol **2013**;15 Suppl 2:ii1-56 doi 10.1093/neuonc/not151.
2. Louis DN, Ohgaki H, Wiestler OD, Cavenee WK, Burger PC, Jouvet A*, et al.* The 2007 WHO classification of tumours of the central nervous system. Acta Neuropathol **2007**;114(2):97-109 doi 10.1007/s00401-007-0243-4.
3. Chan TSY, Wang, X., Spence, T., Taylor, M.D., Huang, A. Embryonal brain tumors. New York: Springer **2015**.
4. Northcott PA, Buchhalter I, Morrissy AS, Hovestadt V, Weischenfeldt J, Ehrenberger T*, et al.* The whole-genome landscape of medulloblastoma subtypes. Nature **2017**;547(7663):311-7 doi 10.1038/nature22973.
5. Picard D, Miller S, Hawkins CE, Bouffet E, Rogers HA, Chan TS*, et al.* Markers of survival and metastatic potential in childhood CNS primitive neuro-ectodermal brain tumours: an integrative genomic analysis. Lancet Oncol **2012**;13(8):838-48 doi 10.1016/S1470-2045(12)70257-7.
6. Sturm D, Orr BA, Toprak UH, Hovestadt V, Jones DTW, Capper D*, et al.* New Brain Tumor Entities Emerge from Molecular Classification of CNS-PNETs. Cell **2016**;164(5):1060-72 doi 10.1016/j.cell.2016.01.015.
7. Tronche F, Kellendonk C, Kretz O, Gass P, Anlag K, Orban PC*, et al.* Disruption of the glucocorticoid receptor gene in the nervous system results in reduced anxiety. Nat Genet **1999**;23(1):99-103 doi 10.1038/12703.
8. Collier LS, Carlson CM, Ravimohan S, Dupuy AJ, Largaespada DA. Cancer gene discovery in solid tumours using transposon-based somatic mutagenesis in the mouse. Nature **2005**;436(7048):272-6 doi 10.1038/nature03681.
9. Dupuy AJ, Akagi K, Largaespada DA, Copeland NG, Jenkins NA. Mammalian mutagenesis using a highly mobile somatic Sleeping Beauty transposon system. Nature **2005**;436(7048):221-6 doi 10.1038/nature03691.
10. Dupuy AJ, Rogers LM, Kim J, Nannapaneni K, Starr TK, Liu P*, et al.* A modified sleeping beauty transposon system that can be used to model a wide variety of human cancers in mice. Cancer Res **2009**;69(20):8150-6 doi 10.1158/0008-5472.CAN-09-1135.
11. Olive KP, Tuveson DA, Ruhe ZC, Yin B, Willis NA, Bronson RT*, et al.* Mutant p53 gain of function in two mouse models of Li-Fraumeni syndrome. Cell **2004**;119(6):847-60 doi 10.1016/j.cell.2004.11.004.
12. Xiao A, Yin C, Yang C, Di Cristofano A, Pandolfi PP, Van Dyke T. Somatic induction of Pten loss in a preclinical astrocytoma model reveals major roles in disease progression and avenues for target discovery and validation. Cancer Res **2005**;65(12):5172-80 doi 10.1158/0008-5472.CAN-04-3902.

13. Rahrmann EP, Watson AL, Keng VW, Choi K, Moriarity BS, Beckmann DA, *et al.* Forward genetic screen for malignant peripheral nerve sheath tumor formation identifies new genes and pathways driving tumorigenesis. Nat Genet **2013**;45(7):756-66 doi 10.1038/ng.2641.
14. Sarver AL, Erdman J, Starr T, Largaespada DA, Silverstein KA. TAPDANCE: an automated tool to identify and annotate transposon insertion CISs and associations between CISs from next generation sequence data. BMC Bioinformatics **2012**;13:154 doi 10.1186/1471-2105-13-154.
15. Temiz NA, Moriarity BS, Wolf NK, Riordan JD, Dupuy AJ, Largaespada DA, *et al.* RNA sequencing of Sleeping Beauty transposon-induced tumors detects transposon-RNA fusions in forward genetic cancer screens. Genome Res **2016**;26(1):119-29 doi 10.1101/gr.188649.114.
16. Scott MC, Temiz NA, Sarver AE, LaRue RS, Rathe SK, Varshney J, *et al.* Comparative Transcriptome Analysis Quantifies Immune Cell Transcript Levels, Metastatic Progression, and Survival in Osteosarcoma. Cancer Res **2018**;78(2):326-37 doi 10.1158/0008-5472.CAN-17-0576.
17. Rack PG, Ni J, Payumo AY, Nguyen V, Crapster JA, Hovestadt V, *et al.* Arhgap36-dependent activation of Gli transcription factors. Proc Natl Acad Sci U S A **2014**;111(30):11061-6 doi 10.1073/pnas.1322362111.
18. Marko TA, Shamsan GA, Edwards EN, Hazelton PE, Rathe SK, Cornax I, *et al.* Slit-Robo GTPase-Activating Protein 2 as a metastasis suppressor in osteosarcoma. Sci Rep **2016**;6:39059 doi 10.1038/srep39059.
19. Yang ZJ, Ellis T, Markant SL, Read TA, Kessler JD, Bourboulas M, *et al.* Medulloblastoma can be initiated by deletion of Patched in lineage-restricted progenitors or stem cells. Cancer Cell **2008**;14(2):135-45 doi 10.1016/j.ccr.2008.07.003.
20. Zuckermann M, Hovestadt V, Knobbe-Thomsen CB, Zapatka M, Northcott PA, Schramm K, *et al.* Somatic CRISPR/Cas9-mediated tumour suppressor disruption enables versatile brain tumour modelling. Nat Commun **2015**;6:7391 doi 10.1038/ncomms8391.
21. Northcott PA, Shih DJ, Peacock J, Garzia L, Morrissy AS, Zichner T, *et al.* Subgroup-specific structural variation across 1,000 medulloblastoma genomes. Nature **2012**;488(7409):49-56 doi 10.1038/nature11327.
22. Kraus JA, Felsberg J, Tonn JC, Reifenberger G, Pietsch T. Molecular genetic analysis of the TP53, PTEN, CDKN2A, EGFR, CDK4 and MDM2 tumour-associated genes in supratentorial primitive neuroectodermal tumours and glioblastomas of childhood. Neuropathol Appl Neurobiol **2002**;28(4):325-33.
23. Wu X, Northcott PA, Dubuc A, Dupuy AJ, Shih DJ, Witt H, *et al.* Clonal selection drives genetic divergence of metastatic medulloblastoma. Nature **2012**;482(7386):529-33 doi 10.1038/nature10825.
24. Northcott PA, Korshunov A, Witt H, Hielscher T, Eberhart CG, Mack S, *et al.* Medulloblastoma comprises four distinct molecular variants. J Clin Oncol **2011**;29(11):1408-14 doi 10.1200/JCO.2009.27.4324.
25. Lin MH, Lee YH, Cheng HL, Chen HY, Jhuang FH, Chueh PJ. Capsaicin Inhibits Multiple Bladder Cancer Cell Phenotypes by Inhibiting Tumor-Associated NADH Oxidase (tNOX) and Sirtuin1 (SIRT1). Molecules **2016**;21(7) doi 10.3390/molecules21070849.
26. Snyder EY, Deitcher DL, Walsh C, Arnold-Aldea S, Hartweieg EA, Cepko CL. Multipotent Neural Cell Lines Can Engraft and Participate in Development of Mouse Cerebellum. Cell **1992**;68:33-51.
27. Eccles RL, Czajkowski MT, Barth C, Muller PM, McShane E, Grunwald S, *et al.* Bimodal antagonism of PKA signalling by ARHGAP36. Nat Commun **2016**;7:12963 doi 10.1038/ncomms12963.
28. Holterman CE, Le Grand F, Kuang S, Seale P, Rudnicki MA. Megf10 regulates the progression of the satellite cell myogenic program. J Cell Biol **2007**;179(5):911-22 doi 10.1083/jcb.200709083.
29. Li X, Wang W, Xi Y, Gao M, Tran M, Aziz KE, *et al.* FOXR2 Interacts with MYC to Promote Its Transcriptional Activities and Tumorigenesis. Cell Rep **2016**;16(2):487-97 doi 10.1016/j.celrep.2016.06.004.
30. Lin JR, Mondal AM, Liu R, Hu J. Minimalist ensemble algorithms for genome-wide protein localization prediction. BMC Bioinformatics **2012**;13:157 doi 10.1186/1471-2105-13-157.
31. Zerbino DR, Achuthan P, Akanni W, Amode MR, Barrell D, Bhai J, *et al.* Ensembl 2018. Nucleic Acids Res **2018**;46(D1):D754-D61 doi 10.1093/nar/gkx1098.
32. Genovesi LA, Ng CG, Davis MJ, Remke M, Taylor MD, Adams DJ, *et al.* Sleeping Beauty mutagenesis in a mouse medulloblastoma model defines networks that discriminate between human molecular subgroups. Proc Natl Acad Sci U S A **2013**;110(46):E4325-34 doi 10.1073/pnas.1318639110.
33. Lastowska M, Al-Afghani H, Al-Balool HH, Sheth H, Mercer E, Coxhead JM, *et al.* Identification of a neuronal transcription factor network involved in medulloblastoma development. Acta Neuropathol Commun **2013**;1:35 doi 10.1186/2051-5960-1-35.
34. Koso H, Tsuhako A, Lyons E, Ward JM, Rust AG, Adams DJ, *et al.* Identification of FoxR2 as an oncogene in medulloblastoma. Cancer Res **2014**;74(8):2351-61 doi 10.1158/0008-5472.CAN-13-1523.

35. Ortiz B, Fabius AW, Wu WH, Pedraza A, Brennan CW, Schultz N*, et al.* Loss of the tyrosine phosphatase PTPRD leads to aberrant STAT3 activation and promotes gliomagenesis. Proc Natl Acad Sci U S A **2014**;111(22):8149-54 doi 10.1073/pnas.1401952111.
36. Dali R, Verginelli F, Pramatarova A, Sladek R, Stifani S. Characterization of a FOXG1:TLE1 transcriptional network in glioblastoma initiating cells. Mol Oncol **2018** doi 10.1002/1878-0261.12168.
37. Fontebasso AM, Schwartzentruber J, Khuong-Quang DA, Liu XY, Sturm D, Korshunov A*, et al.* Mutations in SETD2 and genes affecting histone H3K36 methylation target hemispheric high-grade gliomas. Acta Neuropathol **2013**;125(5):659-69 doi 10.1007/s00401-013-1095-8.
38. Murtaza M, Jolly LA, Gecz J, Wood SA. La FAM fatale: USP9X in development and disease. Cell Mol Life Sci **2015**;72(11):2075-89 doi 10.1007/s00018-015-1851-0.
39. Cianfanelli V, Fuoco C, Lorente M, Salazar M, Quondamatteo F, Gherardini PF*, et al.* AMBRA1 links autophagy to cell proliferation and tumorigenesis by promoting c-Myc dephosphorylation and degradation. Nat Cell Biol **2015**;17(1):20-30 doi 10.1038/ncb3072.
40. Modzelewska K, Boer EF, Mosbruger TL, Picard D, Anderson D, Miles RR*, et al.* MEK Inhibitors Reverse Growth of Embryonal Brain Tumors Derived from Oligoneural Precursor Cells. Cell Rep **2016**;17(5):1255-64 doi 10.1016/j.celrep.2016.09.081.
41. Katoh M, Igarashi M, Fukuda H, Nakagama H, Katoh M. Cancer genetics and genomics of human FOX family genes. Cancer Lett **2013**;328(2):198-206 doi 10.1016/j.canlet.2012.09.017.
42. Liu X, Liu N, Yue C, Wang D, Qi Z, Tu Y*, et al.* FoxR2 promotes glioma proliferation by suppression of the p27 pathway. Oncotarget **2017**;8(34):56255-66 doi 10.18632/oncotarget.17447.
43. Wang X, He B, Gao Y, Li Y. FOXR2 contributes to cell proliferation and malignancy in human hepatocellular carcinoma. Tumour Biol **2016**;37(8):10459-67 doi 10.1007/s13277-016-4923-3.
44. Lu SQ, Qiu Y, Dai WJ, Zhang XY. FOXR2 Promotes the Proliferation, Invasion, and Epithelial-Mesenchymal Transition in Human Colorectal Cancer Cells. Oncol Res **2017**;25(5):681-9 doi 10.3727/096504016X14771034190471.
45. Xu W, Chang J, Liu G, Du X, Li X. Knockdown of FOXR2 suppresses the tumorigenesis, growth and metastasis of prostate cancer. Biomed Pharmacother **2017**;87:471-5 doi 10.1016/j.biopha.2016.12.120.
46. D'Cruz CM, Gunther EJ, Boxer RB, Hartman JL, Sintasath L, Moody SE*, et al.* c-MYC induces mammary tumorigenesis by means of a preferred pathway involving spontaneous Kras2 mutations. Nat Med **2001**;7(2):235-9 doi 10.1038/84691.
47. Sulzmaier FJ, Jean C, Schlaepfer DD. FAK in cancer: mechanistic findings and clinical applications. Nat Rev Cancer **2014**;14(9):598-610 doi 10.1038/nrc3792.
48. Xu B, Lefringhouse J, Liu Z, West D, Baldwin LA, Ou C*, et al.* Inhibition of the integrin/FAK signaling axis and c-Myc synergistically disrupts ovarian cancer malignancy. Oncogenesis **2017**;6(1):e295 doi 10.1038/oncsis.2016.86.
49. Dong X, Wang C, Chen Z, Zhao W. Overcoming the resistance mechanisms of Smoothened inhibitors. Drug Discov Today **2018** doi 10.1016/j.drudis.2018.01.012.

Figure 1.
SB-induced medulloblastoma and CNS-PNET resemble human tumors.
A, Macroscopic images of normal brain and brains with *SB*-induced cerebellar medulloblastoma and CNS-PNET in the cerebral cortex and olfactory bulbs. T=tumor. **B,** Medulloblastoma and CNS-PNET frequency across genetic backgrounds. **C**, Upper panels: medulloblastoma H&E. **i**, Rosettes (arrows), mitotic nuclei (arrowheads). Primary medulloblastoma (T) with leptomeningeal spread (LS). Lower panels: medulloblastoma IHC. **D**, Upper panels: CNS-PNET H&E. Cerebral cortex (ctx), hippocampal formation (hpf), dentate gyrus (dg). Inset: CNS-PNET sagittal section, olfactory bulb (arrow). **ii**, Bulk tumor with rosette formations (arrows) and mitotic nuclei (arrowheads). **iii**, Tumor cell parenchyma infiltration. Lower panels: CNS-PNET IHC. Scale bars = 50 μm.

Figure 2.
SB-induced tumors resemble human medulloblastoma and CNS-PNET transcriptionally.
A, Hierarchical clustering of medulloblastoma transcription profiles(6). Red and green boxes denote transcripts in SHH and group 3/4, respectively (*P*-value <0.002, Fisher's Exact Test (FET)). SHH, WNT, and group 3/4 designation indicated with red, black, and green toebars, respectively. **B**, Hierarchical clustering of CNS-PNET transcription profiles(6). Blue boxes denote transcripts in CNS NB-*FOXR2* (*P*-value <1.0e-8, FET). CNS NB-*FOXR2* and non-*FOXR2* CNS-PNET designation are shown with blue and black toebars, respectively. Log-transformed and mean-centered data with variance >0.5 for murine RNA-Seq datasets and >2.0 for human array datasets were clustered using average linkage clustering. Clusters systematically identified with node correlation >0.2.

Figure 3.
CIS gene identification and expression analysis in mouse and human tumors.
A, Medulloblastoma (MB) and CNS-PNET CIS genes. **B**, RNA-Seq expression levels in *SB*-induced tumors (Student *t* test, two-tailed). **C**-**E**, Expression of CIS genes with highest variability in mouse tumors(**C**), human medulloblastoma(5)(**D**), and human CNS-PNET(5)(**E**). Log-transformed and mean-centered data with variance >1.0 were clustered using average linkage clustering. Multiple human probes corresponding to CIS were averaged to obtain a single value.

Figure 4.
Increased *Arhgap36* expression is associated with medulloblastoma.
A, *Arhgap36* locus with transposon insertions (green arrowheads). **B**, *Arhgap36* expression by RNA-Seq in *SB*-induced medulloblastomas (Student *t* test, two-tailed). **C**, Arhgap36 IHC in *SB*-induced medulloblastoma. Primary tumor (*), leptomeningeal spread (arrowhead). Nuclear expression in control tumor (arrow) compared to normal granule neural cells (inset). **D**, Combined TMAs analyzed for ARHGAP36 by IHC. **E**, ARHGAP36 positivity by IHC across subgrouped Johns Hopkins TMA. **F**, Kaplan-Meier analysis of patients from Johns Hopkins TMA (Log rank Mantel-Cox test). Scale bars = 50mm.

Figure 5.
ARHGAP36 and Megf10 promote tumorigenesis.
A, Soft agar assay comparing C17.2 Luc and C17.2 ARHGAP36 (Student *t* test, two-tailed). **B**, Flank tumor volume of NU/J mice injected with C17.2 Luc or C17.2 ARHGAP36 (N=5, Sidak's multiple comparisons test). **C**, Survival of NU/J mice injected intracranially with C17.2 Luc or C17.2 ARHGAP36 (N=7, Log rank Mantel-Cox test). **D**, IHC showing cerebellar and cerebral location of GFP+ C17.2 Luc or C17.2 ARHGAP36 injected into NU/J mice. **E**, Tritiated thymidine (^{3}H-Td) incorporation assay in transduced GNPs (N=3, Benjamini, Krieger, and Yekutieli multiple comparisons test). **F**, Upper panel: qRT-PCR for *Gli1* in C17.2 Luc and C17.2 ARHGAP36 (Sidak's multiple comparison's test). *Gli1* expression is normalized to *Gapdh*. Lower panel: RNA-Seq of *SB*-induced medulloblastomas showing expression of indicated genes. **G**, MTS assay of C17.2 Luc and C17.2 Megf10 (Sidak's multiple comparisons test). **H**, Soft agar assay of C17.2 Luc and C17.2 Megf10 (Student *t* test, two-tailed). **I**, Flank tumor volume of NU/J mice injected with C17.2 Luc (N=7) or C17.2 Megf10 (N=8)(Sidak's multiple comparisons test). Error bars, SEM. Scale bars = 100mm.

Figure 6.

FOXR2 promotes transformation in human and mouse cells.
A, Transposon insertions (green arrowheads) in the *Foxr2* locus. **B**, *Foxr2* expression by RNA-Seq in *SB*-induced medulloblastoma (Student *t* test, two-tailed). **C**, Western blot showing FOXR2 expression in C17.2 Luc and C17.2 FOXR2. **D**, Soft agar assay comparing C17.2 Luc and C17.2 FOXR2 (Student *t* test, two-tailed). **E**, Wound closure rate of C17.2 Luc (N=14) and C17.2 FOXR2 (N=15)(Student *t* test, two-tailed). **F**, Flank tumor volume of NU/J mice injected with C17.2 Luc (N=7), C17.2 FOXR2ΔMYC (N=6) or C17.2 FOXR2 (N=8)(Sidak's multiple comparison's test). **G**, Whole and halved brains from NU/J mice injected intracranially with C17.2 FOXR2. Scale bars = 1 cm. **H**, Survival of NU/J mice injected intracranially with C17.2 Luc (N=7) or C17.2 FOXR2 (N=10)(Log rank Mantel-Cox test). **I**, Survival of NRG mice injected intracranially with C17.2 Luc or C17.2 FOXR2 (N=13)(Log rank Mantel-Cox test). **J**, Western blot of Daoy WT, Daoy #21 (FOXR2 KO), Daoy #21+ (FOXR2 KO with rescue *FOXR2* cDNA), and Daoy #22 (has integrated CRISPR/Cas9 vector but no *FOXR2* mutation). **K**, MTS assay of Daoy WT, Daoy #21, Daoy #21+ and Daoy #22 (Dunnett's multiple comparison's test). **L**, Soft agar assay of Daoy WT, Daoy #21, Daoy #21+ and Daoy #22 (Dunnett's multiple comparison's test). Error bars, SEM.

Figure 7.
FOXR2 interacts with C-MYC and N-MYC and activates FAK/SRC signaling.
A, CoIP of endogenous C-MYC with flag-tagged FOXR2 in HSC1λ. **B**, CoIP of V5-tagged C-MYC, L-MYC and N-MYC with flag-tagged FOXR2 in HEK293T. **C**, Western blot showing cycloheximide (CHX)-treated HSC1λ and C17.2 with and without *FOXR2*. CHX treatment (100 ug/ml in DMSO) was done for time indicated. **D**, Upper panel: putative FOXR2 protein domains. Lower panel: soft agar assay of C17.2 Luc or indicated *FOXR2* deletion mutants. Error bars, SEM. **E**, Western blot showing effects of FOXR2 expression changes on FAK/SRC signaling.

Author Manuscript Published OnlineFirst on January 23, 2019; DOI: 10.1158/0008-5472.CAN-18-1261
Author manuscripts have been peer reviewed and accepted for publication but have not yet been edited.

Figure 1

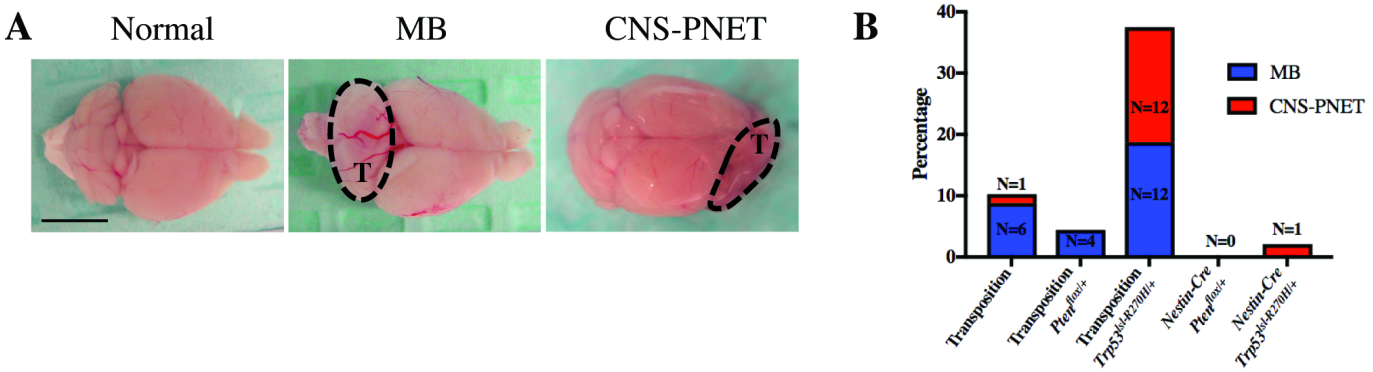

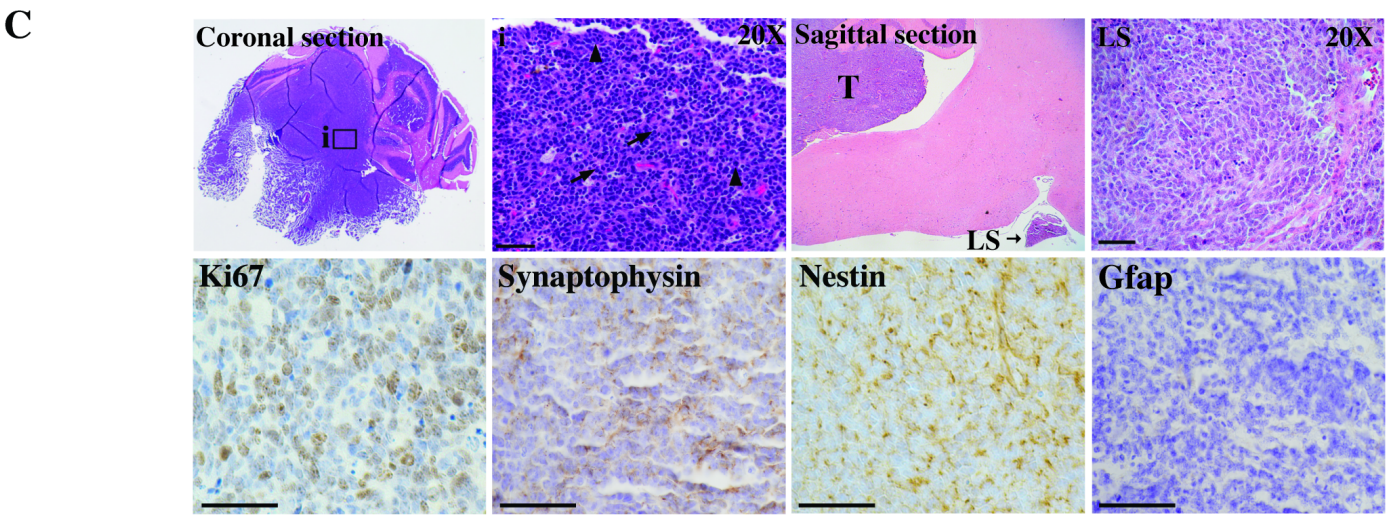

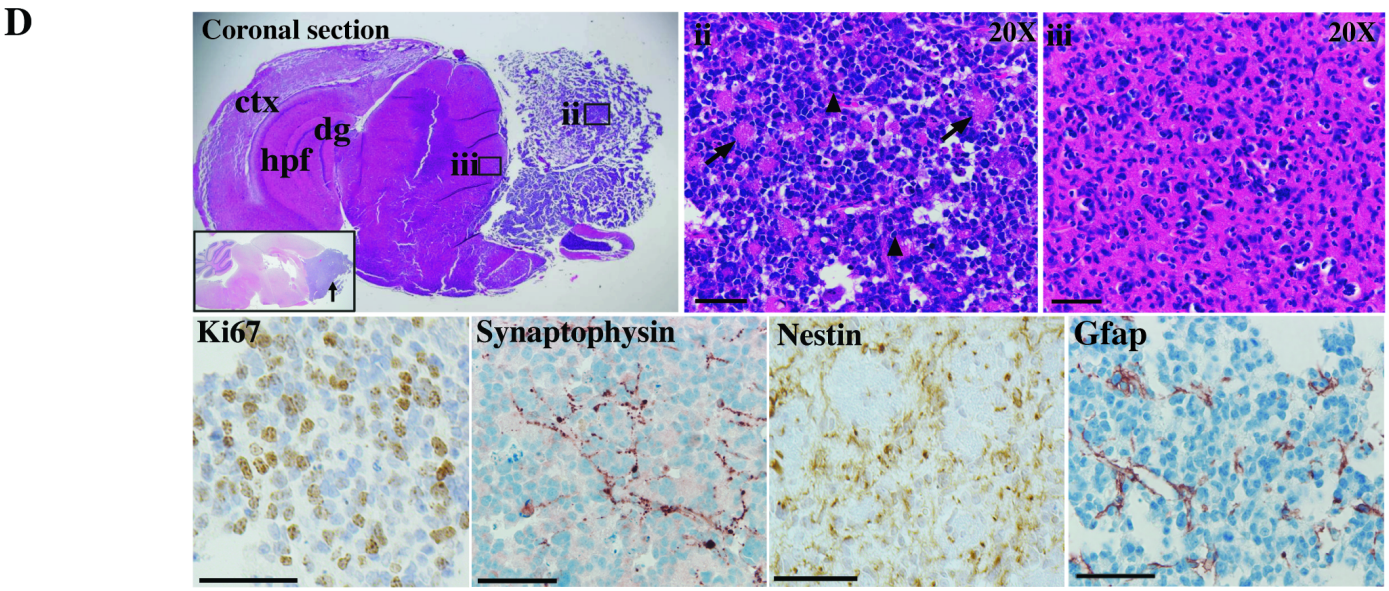

Author Manuscript Published OnlineFirst on January 23, 2019; DOI: 10.1158/0008-5472.CAN-18-1261
Author manuscripts have been peer reviewed and accepted for publication but have not yet been edited.

Figure 2

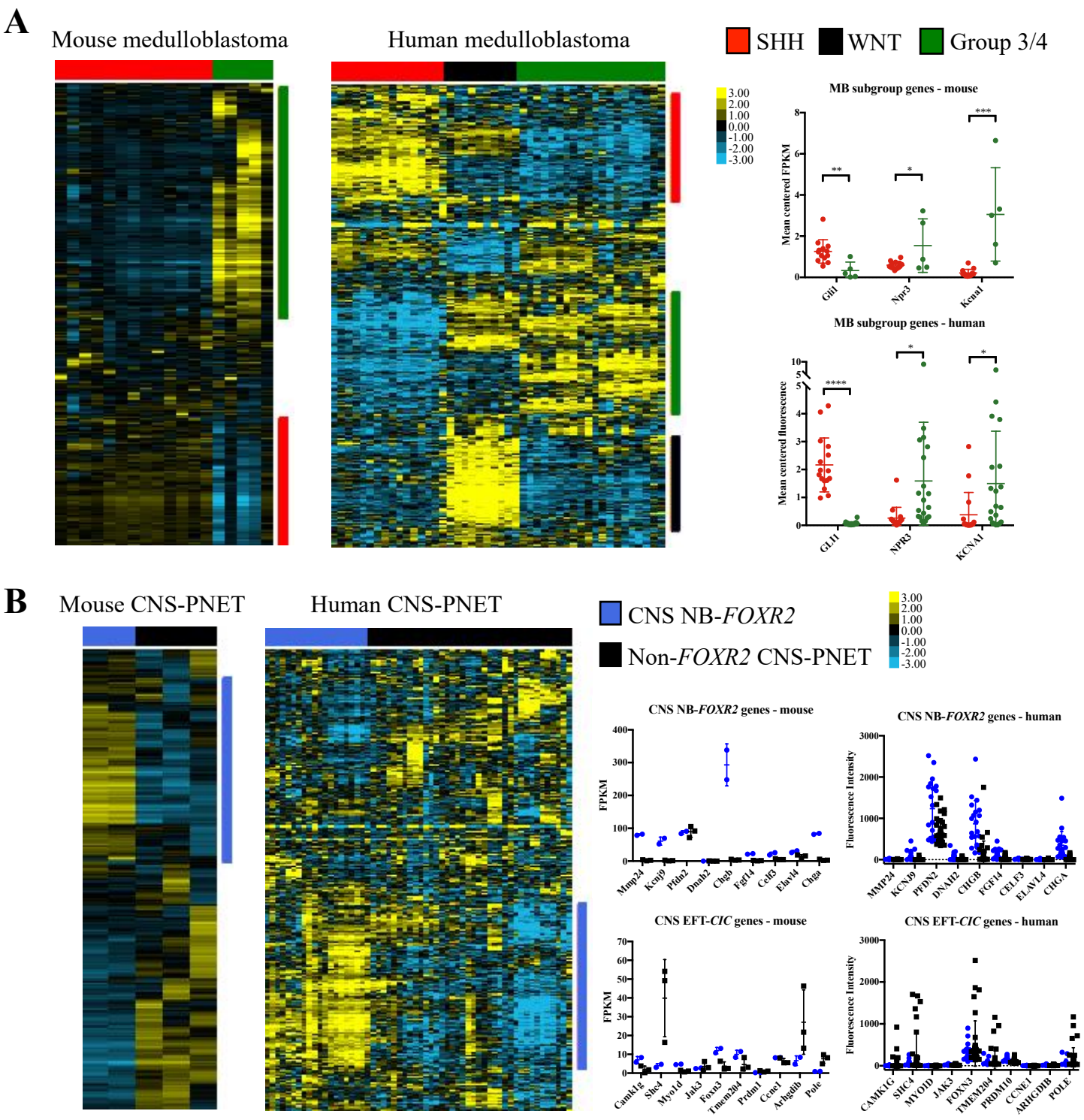

Author Manuscript Published OnlineFirst on January 23, 2019; DOI: 10.1158/0008-5472.CAN-18-1261
Author manuscripts have been peer reviewed and accepted for publication but have not yet been edited.

Figure 3

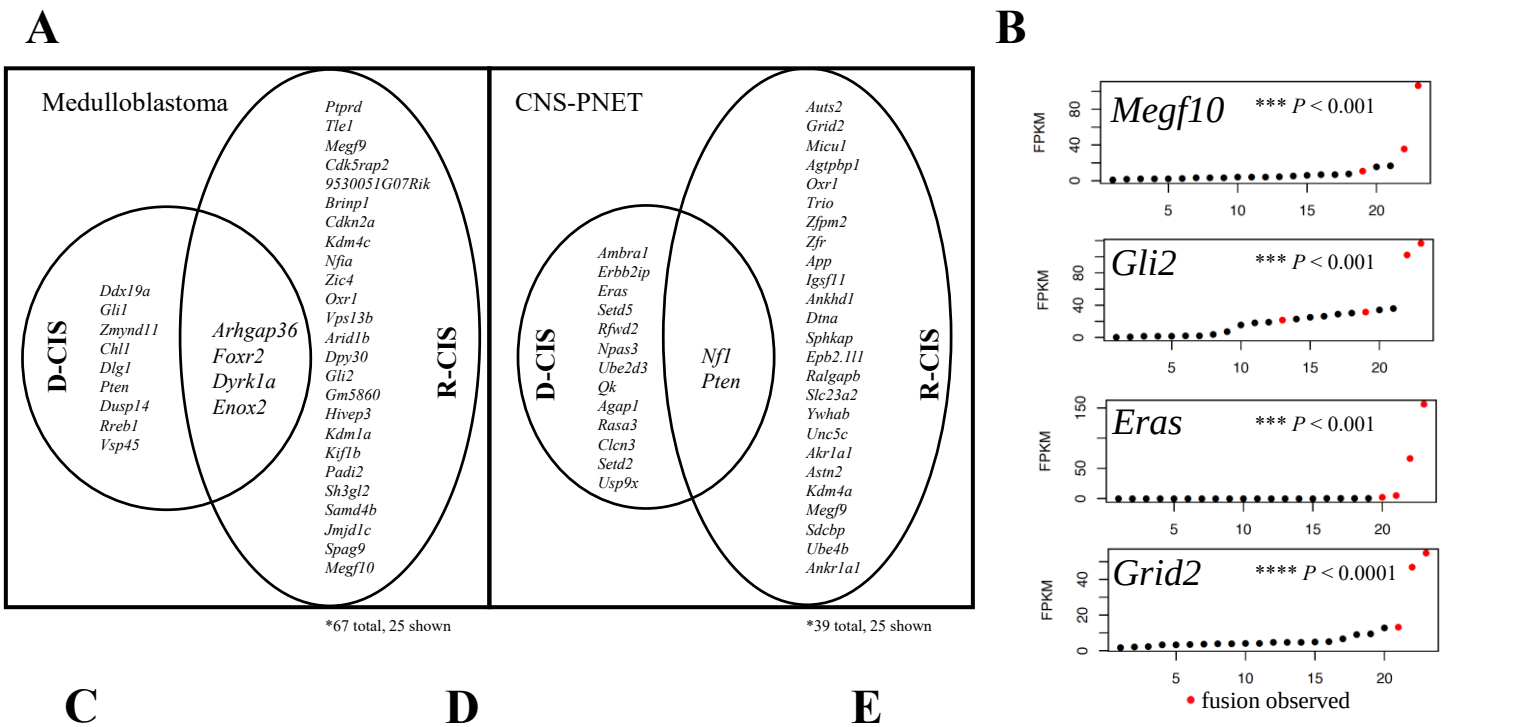

Author Manuscript Published OnlineFirst on January 23, 2019; DOI: 10.1158/0008-5472.CAN-18-1261
Author manuscripts have been peer reviewed and accepted for publication but have not yet been edited.

Figure 4

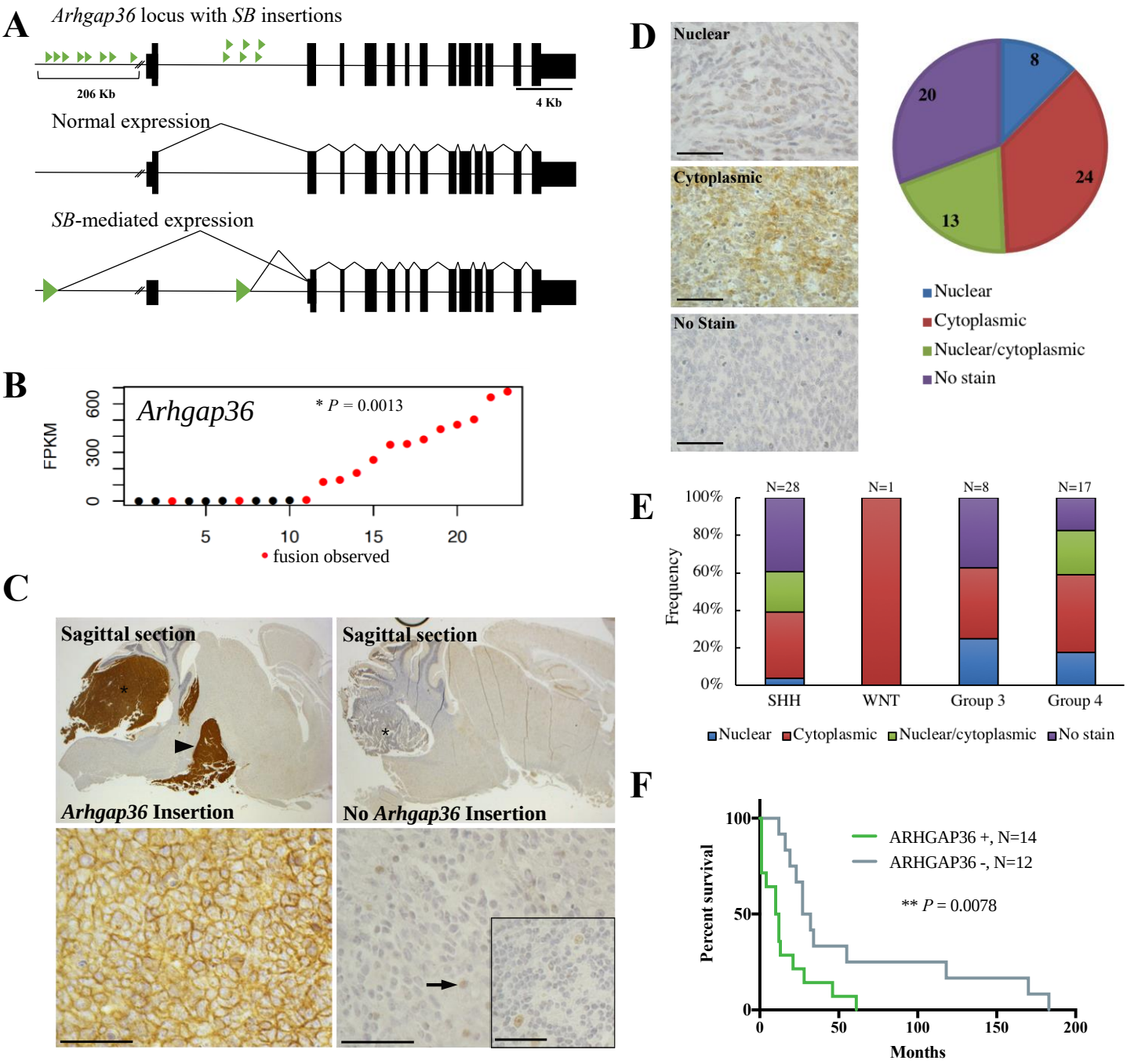

Author Manuscript Published OnlineFirst on January 23, 2019; DOI: 10.1158/0008-5472.CAN-18-1261
Author manuscripts have been peer reviewed and accepted for publication but have not yet been edited.

Figure 5

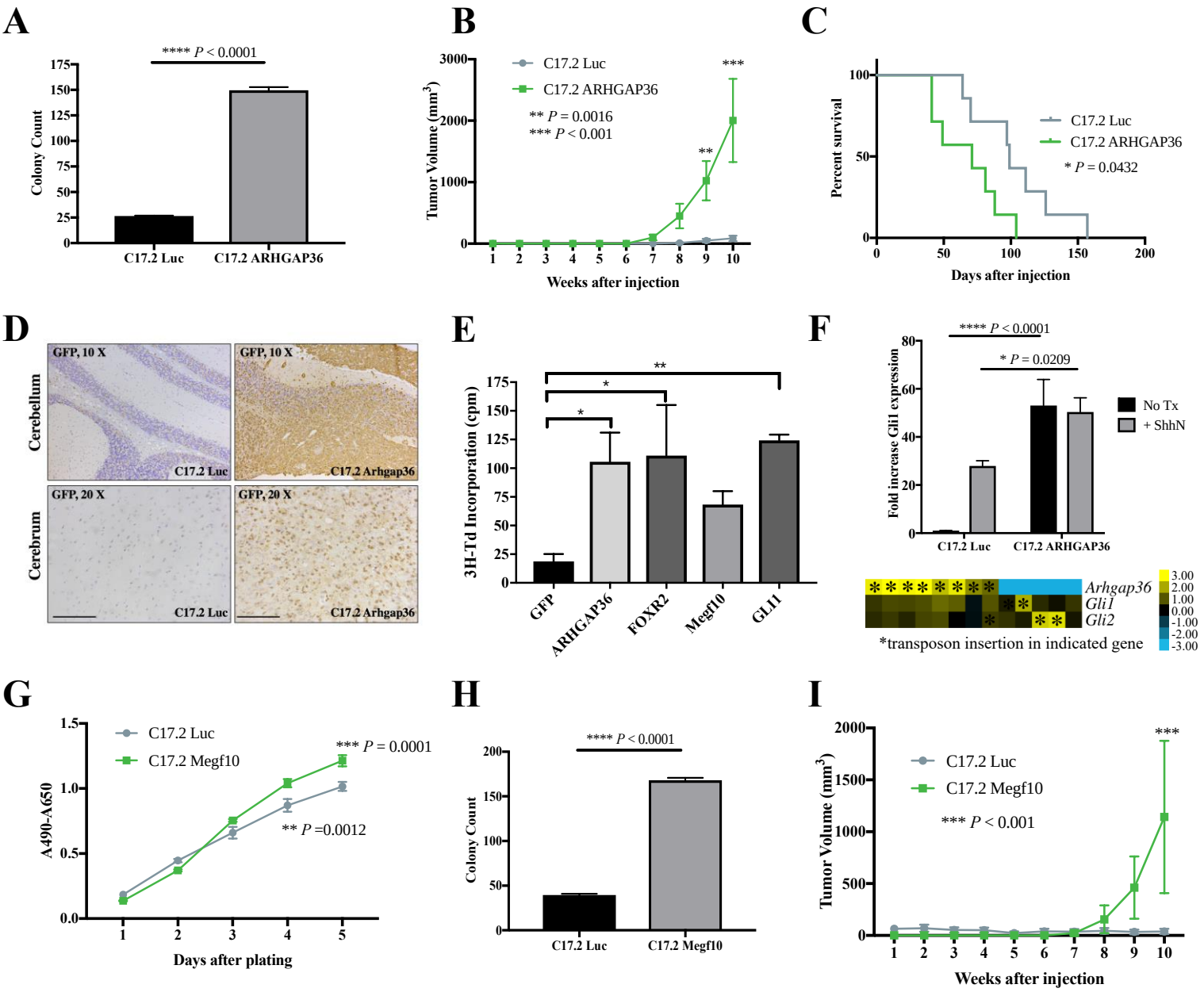

Author Manuscript Published OnlineFirst on January 23, 2019; DOI: 10.1158/0008-5472.CAN-18-1261
Author manuscripts have been peer reviewed and accepted for publication but have not yet been edited.

Figure 6

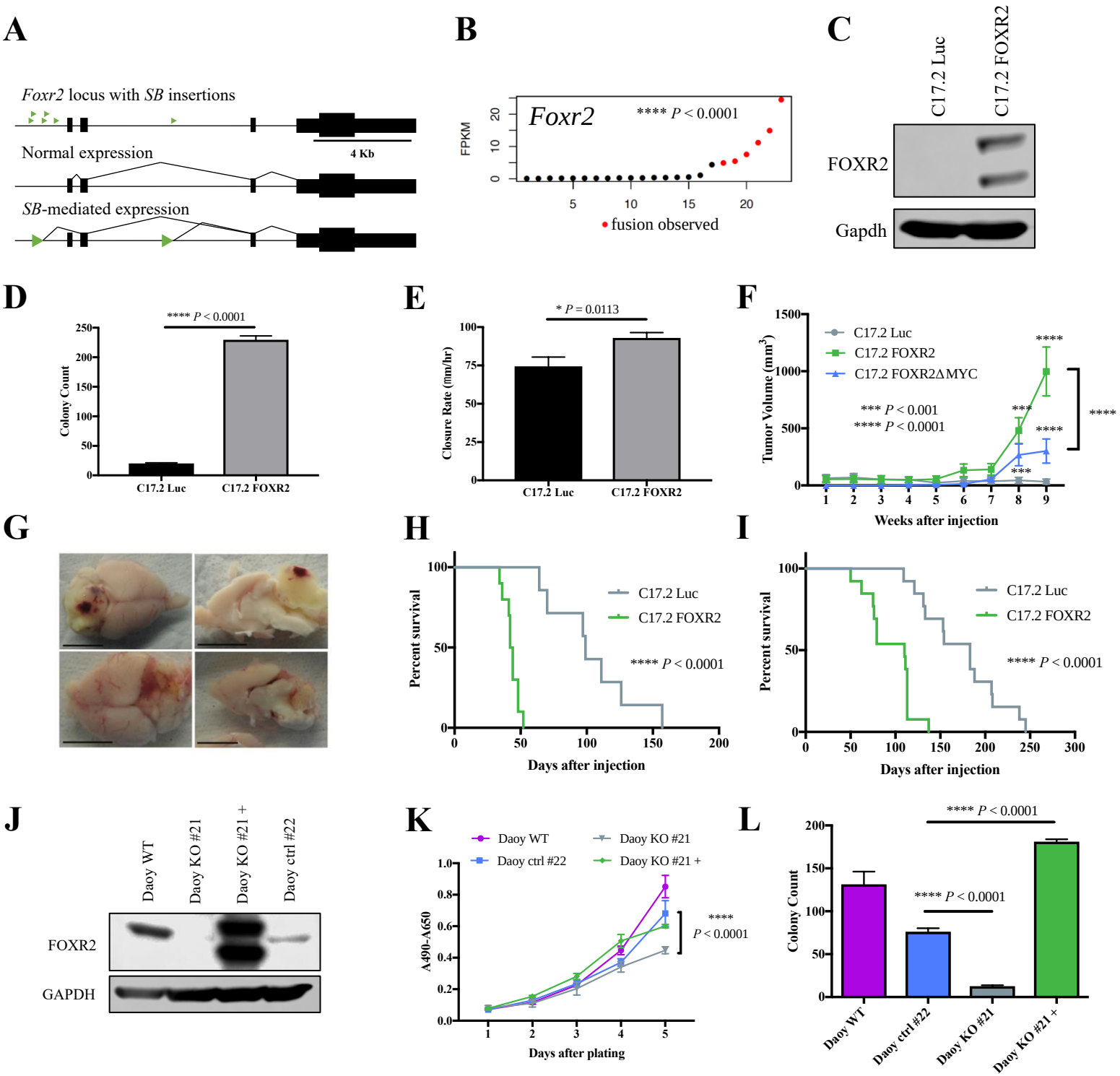

Author Manuscript Published OnlineFirst on January 23, 2019; DOI: 10.1158/0008-5472.CAN-18-1261
Author manuscripts have been peer reviewed and accepted for publication but have not yet been edited.

Figure 7

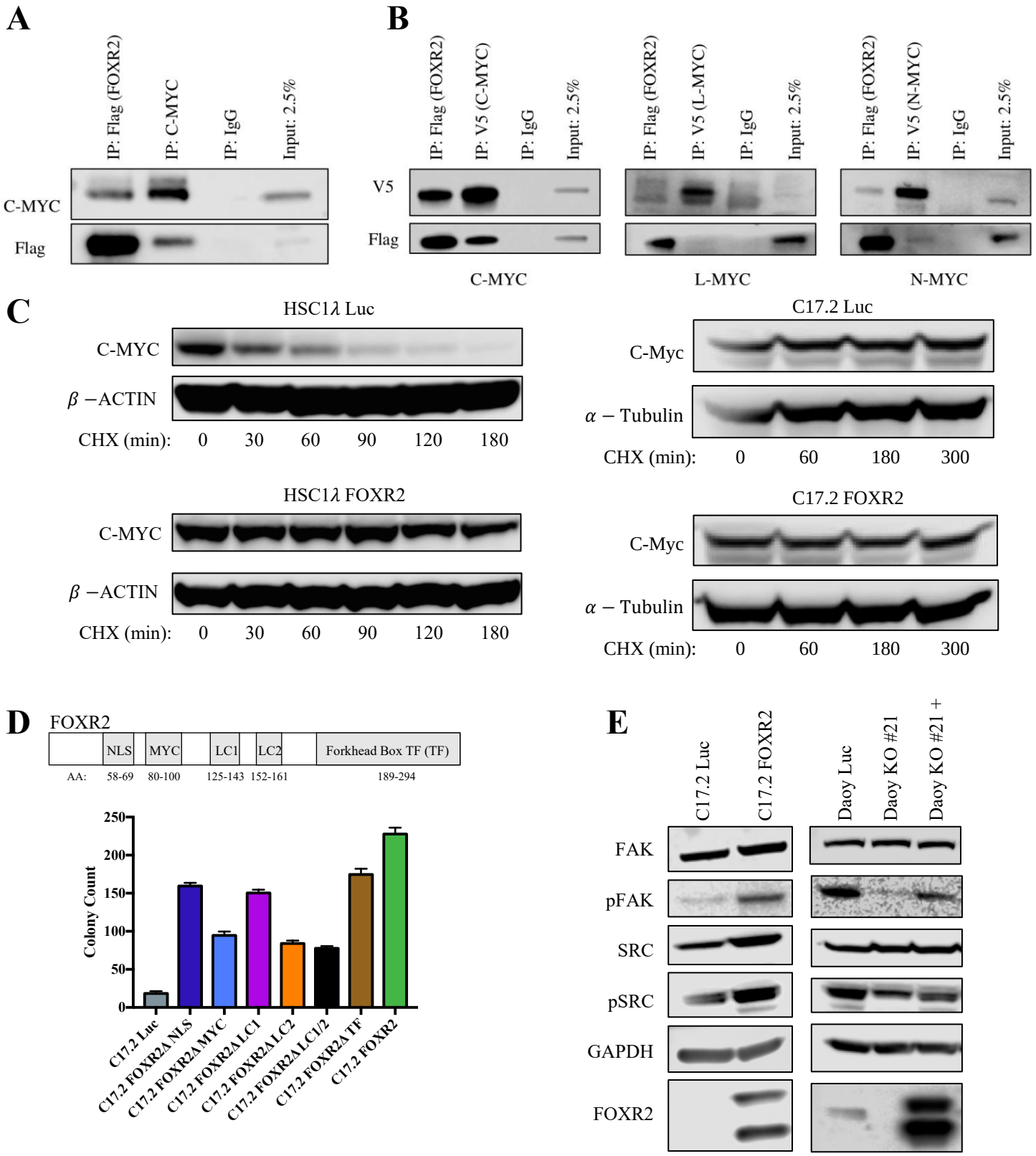

Cancer Research
The Journal of Cancer Research (1916–1930) | The American Journal of Cancer (1931–1940)

AACR American Association for Cancer Research

Sleeping Beauty insertional mutagenesis reveals important genetic drivers of central nervous system embryonal tumors

Pauline J Beckmann, Jon D. Larson, Alex T Larsson, et al.

Cancer Res Published OnlineFirst January 23, 2019.